Photo-production of lowest $\Sigma^*_{1/2^-}$ state within the Regge-effective Lagrangian approach*

Yun-He Lyu (吕云鹤)[1] Han Zhang (张晗)[1] Neng-Chang Wei (韦能昌)[2] Bai-Cian Ke (柯百谦)[1] En Wang (王恩)[1†] Ju-Jun Xie (谢聚军)[3,2,4]

[1]School of Physics and Microelectronics, Zhengzhou University, Zhengzhou 450001, China
[2]School of Nuclear Science and Technology, University of Chinese Academy of Sciences, Beijing 101408, China
[3]Institute of Modern Physics, Chinese Academy of Sciences, Lanzhou 730000, China
[4]Southern Center for Nuclear-Science Theory (SCNT), Institute of Modern Physics, Chinese Academy of Sciences, Huizhou 516000, China

Abstract: Because the lowest Σ^* state with quantum numbers spin-parity $J^P=1/2^-$ is far from being established experimentally and theoretically, we perform a theoretical study on the $\Sigma^*_{1/2^-}$ photo-production within the Regge-effective Lagrangian approach. Considering that $\Sigma^*_{1/2^-}$ couples to the $\bar{K}N$ channel, we study the contributions from the t-channel K exchange diagram. Moreover, the contributions from the t-channel K^* exchange, s-channel nucleon pole, u-channel Σ exchange, and contact term are considered. The differential and total cross sections of the process $\gamma n\to K^+\Sigma^{*-}_{1/2^-}$ are predicted with our model parameters. The results should help in experimentally searching for the $\Sigma^*_{1/2^-}$ state in the future.

Keywords: Σ(1480), effective Lagrangian approach, photoproduction

DOI: 10.1088/1674-1137/acc4ab

I. INTRODUCTION

The study of the low-lying excited Λ^* and Σ^* hyperon resonances is one of the most important issues in hadron physics. In particular, since Λ(1405) was experimentally discovered [1, 2], its nature has garnered significant attention [3–8], and one explanation for Λ(1405) is the $\bar{K}N$ hadronic molecular state [9–15]. In addition, for the isospin $I=1$ partner of Λ(1405), the lowest $\Sigma^*_{1/2^-}$ is crucial to understand light baryon spectra. At present, $\Sigma^*(1620)$ with $J^P=1/2^-$ is listed in the latest version of the Review of Particle Physics (RPP) [16]. It should be emphasized that the $\Sigma^*(1620)$ state is a one-star baryon resonance. Many studies indicate that the lowest $\Sigma^*_{1/2^-}$ resonance is still far from being established, and its mass has been predicted to lie in the range 1380 ~ 1500 MeV [13, 17–20]. Thus, searching for the lowest $\Sigma^*_{1/2^-}$ is helpful for understanding low-lying excited baryons with $J^P=1/2^-$ and light flavor baryon spectra.

The analyses of relevant data on the process $K^-p\to\Lambda\pi^+\pi^-$ suggest that a $\Sigma^*_{1/2^-}$ resonance may exist with a mass of approximately 1380 MeV [17, 18], which is consistent with the predictions of unquenched quark model [21]. The analyses of $K^*\Sigma$ photo-production also indicate that $\Sigma^*_{1/2^-}$ is possibly buried under the $\Sigma^*(1385)$ peak with a mass of 1380 MeV [22], and the search for $\Sigma^*_{1/2^-}$ in the process $\Lambda_c^+\to\eta\pi^+\Lambda$ has been proposed [23]. A more delicate analysis of CLAS data on the process $\gamma p\to K\Sigma\pi$ [24] suggests that the $\Sigma^*_{1/2^-}$ peak should be around 1430 MeV [13]. In Refs. [25, 26], we suggest searching for such a state in the processes $\chi_{c0}(1P)\to\bar{\Sigma}\Sigma\pi$ and $\chi_{c0}(1P)\to\bar{\Lambda}\Sigma\pi$. In addition, in Ref. [27], one $\Sigma^*_{1/2^-}$ state was found with a mass of approximately 1400 MeV by solving coupled channel scattering equations, and Ref. [28] suggests to search for this state in the photo-production process $\gamma p\to K^+\Sigma^{*0}_{1/2^-}$.

It is worth mentioning that a $\Sigma^*(1480)$ resonance with $J^P=1/2^-$ has been listed on the previous version of the RPP [29]. As early as 1970, the $\Sigma^*(1480)$ resonance was

Received 20 January 2023; Accepted 17 March 2023; Published online 18 March 2023

* Supported by the National Natural Science Foundation of China (12192263, 12075288, 11735003, 11961141012), the Natural Science Foundation of Henan (222300420554, 232300421140), the Project of Youth Backbone Teachers of Colleges and Universities of Henan Province (2020GGJS017), the Youth Talent Support Project of Henan (2021HYTP002), the Open Project of Guangxi Key Laboratory of Nuclear Physics and Nuclear Technology (NLK2021-08), and the Youth Innovation Promotion Association CAS

† E-mail: wangen@zzu.edu.cn

reported in the $\Lambda\pi^+$, $\Sigma\pi$, and $p\bar{K}^0$ channels of π^+p scattering in the Princeton-Pennsylvania Accelerator 15-in. hydrogen bubble chamber [30, 31]. In 2004, a bump structure around 1480 MeV was observed in the $K_S^0 p(\bar{p})$ invariant mass spectrum of inclusive deep inelastic ep scattering by the ZEUS Collaboration [32]. Furthermore, a signal for a resonance at 1480 ± 15 MeV with a width of 60 ± 15 MeV was observed in the process $pp\to K^+pY^{*0}$ [33]. $\Sigma^*(1480)$ has been investigated theoretically within different models [34–37]. In Ref. [37], S-wave meson-baryon interactions with strangeness $S=-1$ were studied within the unitary chiral approach, and one narrow pole with a pole position of $1468-\mathrm{i}\,13$ MeV was found in the second Riemann sheet, which may be associated with the $\Sigma^*(1480)$ resonance. However, $\Sigma^*(1480)$ signals are insignificant, and the existence of this state still needs to be confirmed within more precise experimental measurements.

Photo-production reactions have been used to study the excited hyperon states Σ^* and Λ^*, and the LEPS [38] and CLAS [24] Collaborations have accumulated considerable relevant experimental data. For instance, with these data, we analyzed the process $\gamma p\to K\Lambda^*(1405)$ to deepen our understanding of the nature of $\Lambda^*(1405)$ in Ref. [39]. To confirm the existence of $\Sigma^*(1480)$, we propose to investigate the process $\gamma N\to K\Sigma^*(1480)$ [1)] within the Regge-effective Lagrangian approach.

Considering the $\Sigma^*(1480)$ signal was first observed in the $\pi^+\Lambda$ invariant mass distribution of the process $\pi^+p\to\pi^+K^+\Lambda$, and the significance is approximately $3\sim4\sigma$ [31], we search for charged $\Sigma^*(1480)$ in the process $\gamma n\to K^+\Sigma^{*-}_{1/2^-}$, which may also avoid the contributions of possible excited Λ^* states. We consider the t-, s-, and u-channel diagrams in the Born approximation by employing the effective Lagrangian approach, and the t-channel K/K^* exchanges terms within the Regge model. Then, we calculate the differential and total cross sections of the process $\gamma n\to K^+\Sigma^{*-}_{1/2^-}$, which helps the experimental search for $\Sigma^*_{1/2^-}$.

This paper is organized as follows. In Sec. II, the theoretical formalism for studying the $\gamma n\to K^+\Sigma^{*-}(1480)$ reaction is presented. The numerical results of the total and differential cross sections and discussion are shown in Sec. III. Finally, a brief summary is given in the last section.

II. FORMALISM

The reaction mechanisms of the $\Sigma^*(1480)(\equiv\Sigma^*)$ photo-production process are depicted in Fig. 1, where we consider the contributions from the t-channel K and K^* exchange terms, s-channel nucleon pole term, u-channel Σ exchange term, and contact term.

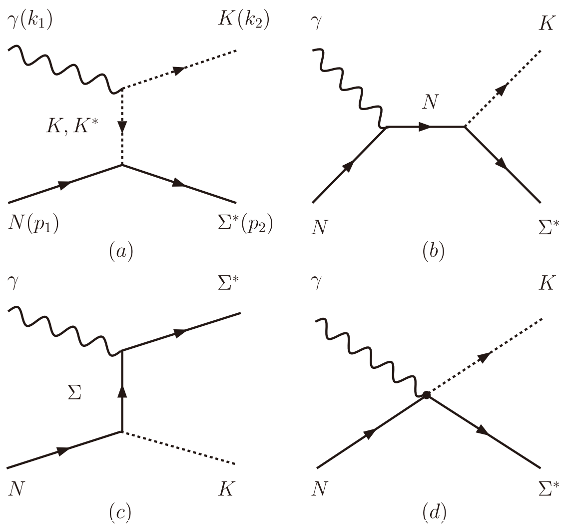

Fig. 1. Mechanisms of the $\gamma n\to K^+\Sigma^{*-}_{1/2^-}$ process. (a) t-channel K/K^* exchange terms, (b) s-channel nuclear term, (c) u-channel Σ exchange term, and (d) contact term. k_1, k_2, p_1, and p_2 represent the four-momenta of the initial photon, kaon, neutron, and $\Sigma^*(1480)$, respectively.

To compute the scattering amplitudes of the Feynman diagrams shown in Fig. 1 within the effective Lagrangian approach, we use the Lagrangian densities for the electromagnetic and strong interaction vertices, as in Refs. [28, 40–45],

$$\mathcal{L}_{\gamma KK}=-\mathrm{i}e\left[K^\dagger\left(\partial_\mu K\right)-\left(\partial_\mu K^\dagger\right)K\right]A^\mu, \tag{1}$$

$$\mathcal{L}_{\gamma KK^*}=g_{\gamma KK^*}\epsilon^{\mu\nu\alpha\beta}\partial_\mu A_\nu\partial_\alpha K^*_\beta K, \tag{2}$$

$$\mathcal{L}_{\gamma NN}=-e\bar{N}\left[\gamma_\mu\hat{e}-\frac{\hat{\kappa}_N}{2M_N}\sigma_{\mu\nu}\partial^\nu\right]A^\mu N, \tag{3}$$

$$\mathcal{L}_{\gamma\Sigma\Sigma^*}=\frac{e\mu_{\Sigma\Sigma^*}}{2M_N}\bar{\Sigma}\gamma_5\sigma_{\mu\nu}\partial^\nu A^\mu\Sigma^*+\text{h.c.}, \tag{4}$$

$$\mathcal{L}_{KN\Sigma}=-\mathrm{i}g_{KN\Sigma}\bar{N}\gamma_5\Sigma K+\text{h.c.}, \tag{5}$$

$$\mathcal{L}_{K^*N\Sigma^*}=\mathrm{i}\frac{g_{K^*N\Sigma^*}}{\sqrt{3}}\bar{K}^{*\mu}\bar{\Sigma}^*\gamma_\mu\gamma_5 N+\text{h.c.}, \tag{6}$$

$$\mathcal{L}_{KN\Sigma^*}=g_{KN\Sigma^*}\bar{K}\bar{\Sigma}^*N+\text{h.c.}, \tag{7}$$

where $e(=\sqrt{4\pi\alpha})$ is the elementary charge unit, A^μ is the photon field, and $\hat{e}\equiv(1+\tau_3)/2$ denotes the charge operator acting on the nucleon field. $\hat{\kappa}_N\equiv\kappa_p\hat{e}+\kappa_n(1-\hat{e})$ is the

1) Here after, we denote $\Sigma^*(1480)$ as the lowest $\Sigma^*_{1/2^-}$ state unless otherwise stated.

anomalous magnetic moment, and we take $\kappa_n = -1.913$ for the neutron [16]. M_N and M_Σ denote the masses of the nucleon and the ground-state of the Σ hyperon, respectively. The strong coupling $g_{KN\Sigma}$ is taken to be 4.09 from Refs. [46–48]. $g_{\gamma KK^*} = 0.254\ \mathrm{GeV}^{-1}$ is determined from the experimental data of $\Gamma_{K^*\to K^*\gamma}$ [16], and the value of $g_{K^*N\Sigma^*} = -3.26 - \mathrm{i}\,0.06$ is taken from Ref. [27]. In addition, the coupling $g_{KN\Sigma^*} = 8.74$ GeV is taken from Ref. [37], and the transition magnetic moment $\mu_{\Sigma\Sigma^*} = 1.28$ is taken from Ref. [28][1)].

In addition to the pseudoscalar coupling of Eq. (5), the vertex of $KN\Sigma$ may be described with the Lagrangian density of axial-vector coupling as follows [49, 50]

$$\mathcal{L}_{KN\Sigma} = -\frac{g_{KN\Sigma}}{2M_N}\bar{N}\gamma_5\gamma_\mu(\partial^\mu K)\Sigma + \mathrm{h.c.}. \tag{8}$$

We discuss the difference between the two schemes in the next section. In this work, we perform the calculations with the Lagrangian density of Eq. (5) for the vertex of $KN\Sigma$ in the following.

With the effective interaction Lagrangian densities given above, the invariant scattering amplitudes are defined as

$$\mathcal{M} = \bar{u}_{\Sigma^*}(p_2, s_{\Sigma^*})\mathcal{M}^\mu_h u_N(k_2, s_p)\epsilon_\mu(k_1, \lambda), \tag{9}$$

where u_{Σ^*} and u_N represent the Dirac spinors, $\epsilon_\mu(k_1,\lambda)$ is the photon polarization vector, and the sub-index h corresponds to the different diagrams of Fig. 1. The reduced amplitudes $\mathcal{M}^\mu_h$ are written as

$$\mathcal{M}^\mu_{K^*} = \frac{g_{\gamma KK^*}g_{K^*N\Sigma^*}}{\sqrt{3}(t-M^2_{K^*})}\epsilon^{\alpha\beta\mu\nu}k_{1\alpha}k_{2\beta}\gamma_\nu\gamma_5, \tag{10}$$

$$\mathcal{M}^\mu_{K^-} = -2\mathrm{i}\frac{eg_{KN\Sigma^*}}{t-M^2_K}k^\mu_2, \tag{11}$$

$$\mathcal{M}^\mu_{\Sigma^-} = -\mathrm{i}\frac{e\mu_{\Sigma\Sigma^*}g_{KN\Sigma}}{2M_n(u-M^2_\Sigma)}(\not{q}_u - M_\Sigma)\sigma^{\mu\nu}k_{1\nu}, \tag{12}$$

$$\mathcal{M}^\mu_n = \frac{\kappa_n g_{KN\Sigma^*}}{2M_n(s-M^2_n)}\sigma^{\mu\nu}k_{1\nu}(\not{q}_s + M_n). \tag{13}$$

To maintain gauge invariance in the full photoproduction amplitudes considered here, we adopt the amplitude of the contact term

$$\mathcal{M}^\mu_c = -\mathrm{i}eg_{KN\Sigma^*}\frac{p^\mu_2}{p_2\cdot k_1}, \tag{14}$$

for $\gamma n \to K^+\Sigma^{*-}_{1/2^-}$.

It is known that the Reggeon exchange mechanism plays a crucial role at high energies and forward angles [51–54]; thus, we adopt the Regge model when modeling the t-channel K and K^* contributions by replacing the usual pole-like Feynman propagator with the corresponding Regge propagators as follows

$$\frac{1}{t-M^2_K} \to \mathcal{F}^{\mathrm{Regge}}_K = \left(\frac{s}{s^K_0}\right)^{\alpha_K(t)}\frac{\pi\alpha'_K}{\sin(\pi\alpha_K(t))\Gamma(1+\alpha_K(t))}, \tag{15}$$

$$\frac{1}{t-M^2_{K^*}} \to \mathcal{F}^{\mathrm{Regge}}_{K^*} = \left(\frac{s}{s^{K^*}_0}\right)^{\alpha_{K^*}(t)-1}\frac{\pi\alpha'_{K^*}}{\sin(\pi\alpha_{K^*}(t))\Gamma(\alpha_{K^*}(t))}, \tag{16}$$

where $\alpha_K(t) = 0.7\ \mathrm{GeV}^{-2}\times(t-M^2_K)$ and $\alpha_{K^*}(t) = 1 + 0.83\ \mathrm{GeV}^{-2}\times(t-M^2_{K^*})$ are the linear Reggeon trajectories. The constants s^K_0 and $s^{K^*}_0$ are determined to be 3.0 GeV^2 and 1.5 GeV^2, respectively [55]. Here, α'_K and α'_{K^*} are the Regge-slopes.

Then, the full photo-production amplitudes for the $\gamma n \to K^+\Sigma^{*-}_{1/2^-}$ reaction can be expressed as

$$\begin{aligned}\mathcal{M}^\mu = &\left(\mathcal{M}^\mu_{K^-} + \mathcal{M}^\mu_c\right)\left(t-M^2_K\right)\mathcal{F}^{\mathrm{Regge}}_K + \mathcal{M}^\mu_{\Sigma^-}f_u \\ &+ \mathcal{M}^\mu_{K^*}\left(t-M^2_{K^*}\right)\mathcal{F}^{\mathrm{Regge}}_{K^*} + \mathcal{M}^\mu_n f_s,\end{aligned} \tag{17}$$

where $\mathcal{F}^{\mathrm{Regge}}_K$ and $\mathcal{F}^{\mathrm{Regge}}_{K^*}$ represent the Regge propagators. The form factors f_s and f_u are included to suppress the large momentum transfer of the intermediate particles and describe their off-shell behavior because the intermediate hadrons are not point-like particles. For s-channel and u-channel baryon exchanges, we use the following form factors [40, 56]

$$f_i(q^2_i) = \left[\frac{\Lambda^4_i}{\Lambda^4_i + (q^2_i - M^2_i)^2}\right]^2, i = s, u \tag{18}$$

where M_i and q_i are the masses and four-momenta of the intermediate baryons, and Λ_i represents the cut-off val-

1) For the vertex of the $K^*N\Sigma^*$, the tensor term is also possible, and the Lagrangian density could be written as

$$\mathcal{L}_{K^*N\Sigma^*} = -\mathrm{i}\frac{g_{K^*N\Sigma^*}}{\sqrt{3}}\bar{\Sigma}^*\gamma_5\left(\gamma^\mu - \frac{\kappa_{K^*N\Sigma}}{2M_N}\sigma^{\mu\nu}\partial_\nu\right)K^*_\mu N,$$

where the coupling constant $\kappa_{K^*N\Sigma^*}$ is unknown. Taking into account that the contribution from the t-channel K^* exchange is much small, and there is no information about the parameter $\kappa_{K^*N\Sigma^*}$, we ignore the contribution from the tensor term for the t-channel K^* exchange in this work.

ues for the baryon exchange diagrams. In this study, we take $\Lambda_s = \Lambda_u = 1.5$ GeV and discuss the results with different cut-offs.

Finally, the unpolarized differential cross section in the center of mass (c.m.) frame for the $\gamma n \to K\Sigma^{*-}_{1/2^-}$ reaction reads as

$$\frac{d\sigma}{d\Omega} = \frac{M_N M_{\Sigma^*}|\vec{k}_1^{\text{c.m.}}||\vec{k}_2^{\text{c.m.}}|}{8\pi^2(s-M_N^2)^2} \sum_{\lambda,s_p,s_{\Sigma^*}} |\mathcal{M}|^2, \tag{19}$$

where s denotes the invariant mass square of the center of mass (c.m.) frame for $\Sigma^*_{1/2^-}$ photo-production, and $d\Omega = 2\pi d\cos\theta_{\text{c.m.}}$, with $\theta_{\text{c.m.}}$ as the polar outgoing K scattering angle. Here, $\vec{k}_1^{\text{c.m.}}$ and $\vec{k}_2^{\text{c.m.}}$ are the three-momenta of the photon and K meson in the c.m. frame,

$$|\vec{k}_1^{\text{c.m.}}| = \frac{s-M_N^2}{2\sqrt{s}}, \tag{20}$$

$$|\vec{k}_2^{\text{c.m.}}| = \frac{\sqrt{[s-(M_{\Sigma^*}+M_K)^2][s-(M_{\Sigma^*}-M_K)^2]}}{2\sqrt{s}}. \tag{21}$$

III. NUMERICAL RESULTS AND DISCUSSIONS

In this section, we present our numerical results on the differential and total cross sections for the $\gamma n \to K^+\Sigma^{*-}_{1/2^-}$ reaction. The masses of the mesons and baryons are taken from the RPP [16], as given in Table 1. In addition, the mass and width of $\Sigma^*(1480)$ are $M = 1480 \pm 15$ MeV and $\Gamma = 60 \pm 15$ MeV, respectively [29].

Table 1. Particle masses used in this study.

Particle	Mass/MeV
n	939.565
Σ^-	1197.449
K^+	493.677
K^-	493.677
K^*	891.66

First, we show the angle dependence of the differential cross sections for the $\gamma n \to K^+\Sigma^{*-}_{1/2^-}$ reaction in Fig. 2, where the center-of-mass energies $W = \sqrt{s}$ varies from 2.0 to 2.8GeV. The black curves labeled as "Total" are the results of all the contributions from the t-, s-, and u-channels and the contact term. The blue-dot and red-dashed curves represent the contributions from the u-channel Σ exchange and t-channel K exchange mechanisms, respectively. The magenta-dot-dashed and green-dot curves correspond to the contributions from the s-channel and t-channel K^* exchange diagrams, respectively, whereas the cyan-dot-dashed curves represent the contributions from the contact term. According to the differential cross sections, we find that the t-channel K meson exchange term plays an important role at forward angles for the process $\gamma n \to K^+\Sigma^{*-}_{1/2^-}$, mainly because of the Regge effects of t-channel K exchange. The K-Reggeon exchange exhibits a steadily increasing behavior with $\cos\theta_{\text{c.m.}}$ and falls off drastically at very forward angles, which is consistent with the results of Ref. [28]. In the appendix, we show that the contribution from the t-channel K exchange is zero in the forward angle ($\theta_{\text{c.m.}} = 0$) and the backward angle ($\theta_{\text{c.m.}} = \pi$). In addition, the u-channel Σ exchange term mainly contributes to the backward angles. It should be emphasized that the contribution from the t-channel K^* exchange term is small and can be safely neglected for the process $\gamma n \to K^+\Sigma^{*-}_{1/2^-}$, which is consistent with the results of Ref. [28].

As mentioned in Sec. II, in addition to the pseudoscalar coupling of Eq. (5), the vertex of $KN\Sigma$ may also be described with the Lagrangian density of axial-vector coupling [Eq. (8)]. We also present the contribution from the u-channel Σ exchange with the Lagrangian densities of Eqs. (5) and (8) in Fig. 3; we find that both of them contribute to the backward angles. Because the contribution from the u-channel is small, it is expected that either pseudoscalar coupling or axial-vector coupling for $KN\Sigma$ does not affect our results significantly.

In addition to the differential cross sections, we also calculate the total cross section of the $\gamma n \to K^+\Sigma^{*-}_{1/2^-}$ reaction as a function of the initial photon energy. The results are shown in Fig. 4. The black curve labeled as "Total" represents the results of all the contributions, including the t-, s-, and u-channels and the contact term. The blue-dot and red-dashed curves represent the contributions from the u-channel Σ exchange and t-channel K exchange mechanisms, respectively. The magenta-dot-dashed and green-dot curves represent the contributions of the s-channel and t-channel K^* exchange diagrams, respectively, whereas the cyan-dot-dashed curve represents the contribution of the contact term. For the $\gamma n \to K^+\Sigma^{*-}_{1/2^-}$ reaction, its total cross section attains a maximum value of approximately 4.2 μb at $E_\gamma = 2.4$ GeV. It is expected that $\Sigma^*(1480)$ can be observed by future experiments in the process $\gamma n \to K^+\Sigma^{*-}(1480) \to \Sigma^-\pi^0/\Sigma^0\pi^-/\Sigma^-\gamma$.

Finally, we show the total cross section for $\gamma n \to K^+\Sigma^{*-}_{1/2^-}$ with the cut-off $\Lambda_{s/u} = 1.2$, 1.5, and 1.8 GeV in Fig. 5. We find that the total cross sections are weakly dependent on the value of the cut-off. Because the precise couplings of $\Sigma^*(1480)$ are still unknown, future experiments would benefit from constraining these couplings if the state $\Sigma^*(1480)$ is confirmed.

IV. SUMMARY

The lowest $\Sigma^{*-}_{1/2^-}$ is far from established, and its exist-

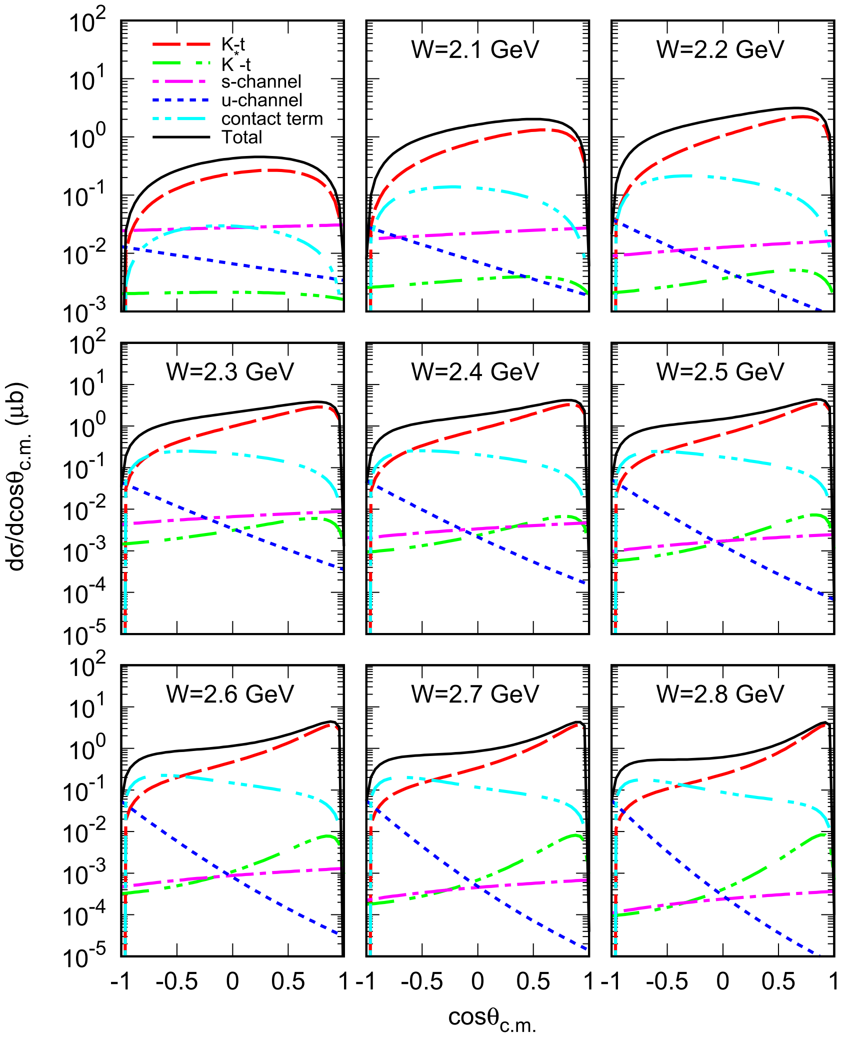

Fig. 2. (color online) $\gamma n \to K^+\Sigma^{*-}_{1/2^-}$ differential cross sections as a function of $\cos\theta_{\rm c.m.}$ are plotted for γn-invariant mass intervals (in GeV units). The black curve labeled as "Total" represent the results of all the contributions, including the t-, s-, and u-channels and the contact term. The blue-dot and red-dashed curves denote the contributions from the effective Lagrangian approach u-channel Σ exchange and t-channel K exchange mechanisms, respectively. The magenta-dot-dashed and green-dot-dashed curves represent the contributions of the s-channel and t-channel K^* exchange diagrams, respectively, whereas the cyan-dot-dashed curves represent the contributions of the contact term.

ence is important to understand low-lying excited baryons with $J^P = 1/2^-$. There are many experimental hints of $\Sigma^*(1480)$, as listed in the previous version of the RPP. We propose to search for this state in the photoproduction process to confirm its existence.

Assuming that the $J^P = 1/2^-$ low lying state $\Sigma^*(1480)$ has a sizeable coupling to $\bar{K}N$ according to the study of Ref. [37], we phenomenologically investigate the $\gamma n \to K^+\Sigma^{*-}_{1/2^-}$ reaction by considering the contributions from the t-channel K/K^* exchange term, s-channel nucleon term, u-channel Σ exchange term, and contact term within the Regge-effective Lagrangian approach. The differential and total cross sections for these processes are calculated with our model parameters. The total cross section of $\gamma n \to K^+\Sigma^{*-}_{1/2^-}$ is approximately 4.2 μb around $E_\gamma = 2.4$ GeV. We encourage our experimental colleagues to further measure the $\gamma n \to K^+\Sigma^{*-}_{1/2^-}$ process.

APPENDIX A: *t*-CHANNEL *K* EXCHANGE IN THE FORWARD/BACKWARD ANGLE

In this appendix, we show that the contributions from the t-channel K exchange in the forward angle ($\theta = 0$) and backward angle ($\theta = \pi$) are zero. In the c.m frame, the four-momenta of the outgoing K are

$$k_2^0 = \frac{s + m_K^2 - M_{\Sigma^*}^2}{2\sqrt{s}}, \tag{A1}$$

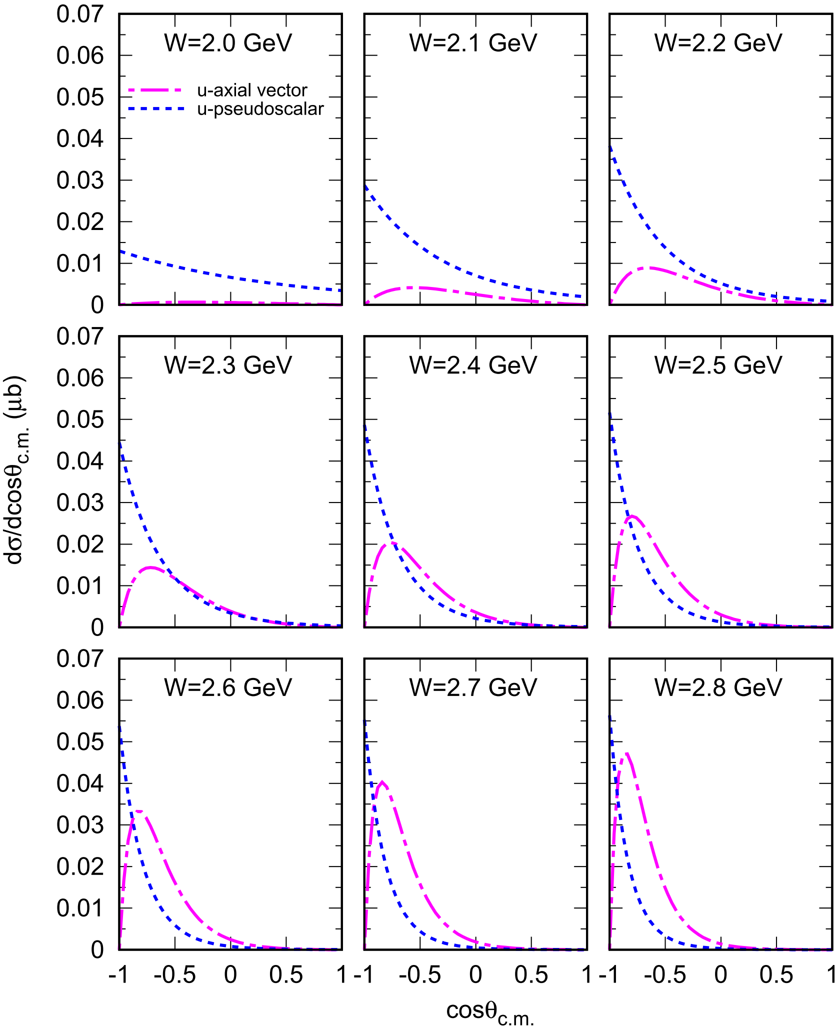

Fig. 3. (color online) $\gamma n \to K^+\Sigma^{*-}_{1/2^-}$ differential cross sections with only the contribution from *u*-channel Σ exchange. The magenta-dot-dashed curves represent the results obtained with the axial-vector coupling of Eq. (8), and the blue-dotted curves represent the results obtained with the pseudoscalar coupling of Eq. (5).

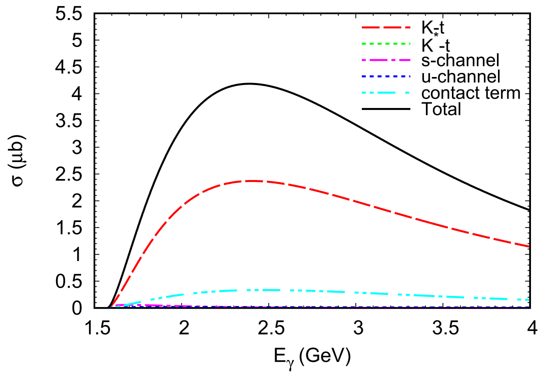

Fig. 4. (color online) Total cross section for $\gamma n \to K^+\Sigma^*_{1/2^-}$ is plotted as a function of the lab energy E_γ. The black curve labeled as "Total" represents the results of all the contributions, including the *t*-, *s*-, and *u*-channels and the contact term. The blue-dot and red-dashed curves represent the contributions from the effective Lagrangian approach *u*-channel Σ exchange and *t*-channel *K* exchange mechanisms, respectively. The magenta-dot-dashed and green-dot curves represent the contributions of the *s*-channel nucleon term and *t*-channel K^* exchange diagrams, respectively, whereas the cyan-dot-dashed curve represents the contribution of the contact term.

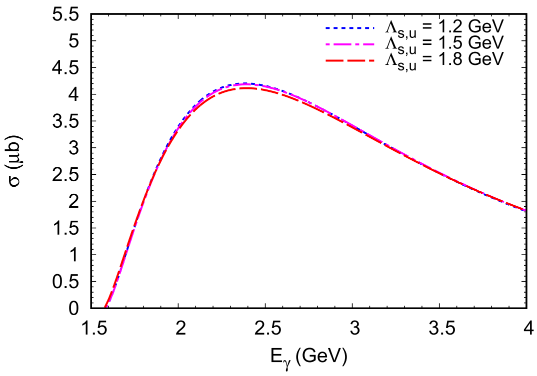

Fig. 5. (color online) Total cross section for $\gamma n \to K^+\Sigma^*_{1/2^-}$ with the cut-off $\Lambda_{s/u} = 1.2$, 1.5, and 1.8 GeV.

$$k_2^1 = |\vec{k}_2^{\text{c.m.}}|\sin\theta, \tag{A2}$$

$$k_2^2 = 0, \tag{A3}$$

$$k_2^3 = |\vec{k}_2^{\text{c.m.}}|\cos\theta, \tag{A4}$$

where $\vec{k}_2^{\text{c.m.}}$ is the three-momentum of K [Eq. (21)]. The polarization vectors of the photon with momentum $\vec{k}_1^{\text{c.m.}}$ in the helicity basis are

$$\epsilon(\vec{k}_1^{\text{c.m.}}, \lambda = \pm 1) = \pm\frac{1}{\sqrt{2}}\begin{pmatrix} 0 \\ 1 \\ \mp\text{i} \\ 0 \end{pmatrix}, \tag{A5}$$

$$\epsilon(\vec{k}_1^{\text{c.m.}}, \lambda = 0) = 0. \tag{A6}$$

We can easily find that $k_2^\mu \epsilon_\mu(\vec{k}_1^{\text{c.m.}}, \lambda = 0, \pm 1) = 0$ for $\theta = 0, \pi$, which implies that the amplitude of Eq. (11) for t-channel K exchange will be zero in the forward angle ($\theta = 0$) and backward angle ($\theta = \pi$).

References

[1] R. H. Dalitz and S. F. Tuan, Phys. Rev. Lett. **2**, 425-428 (1959)
[2] M. H. Alston, L. W. Alvarez, P. Eberhard *et al.*, Phys. Rev. Lett. **6**, 698-702 (1961)
[3] J. A. Oller and U. G. Meissner, Phys. Lett. B **500**, 263-272 (2001)
[4] D. Jido, J. A. Oller, E. Oset *et al.*, Nucl. Phys. A **725**, 181-200 (2003)
[5] N. Isgur and G. Karl, Phys. Rev. D **18**, 4187 (1978)
[6] S. Capstick and N. Isgur, Phys. Rev. D **34**(9), 2809-2835 (1986)
[7] A. Zhang, Y. R. Liu, P. Z. Huang *et al.*, HEP&NP **29**, 250 (2005)
[8] C. G. Callan, Jr. and I. R. Klebanov, Nucl. Phys. B **262**, 365-382 (1985)
[9] E. Oset and A. Ramos, Nucl. Phys. A **635**, 99-120 (1998)
[10] T. Hyodo, S. I. Nam, Phys. Rev. C **68**, 018201 (2003)
[11] T. Hyodo and D. Jido, Prog. Part. Nucl. Phys. **67**, 55-98 (2012)
[12] Z. H. Guo and J. A. Oller, Phys. Rev. C **87**(3), 035202 (2013)
[13] L. Roca and E. Oset, Phys. Rev. C **88**(5), 055206 (2013)
[14] J. X. Lu, L. S. Geng, M. Doering *et al.*, Phys. Rev. Lett. **130**(7), 071902 (2023)
[15] D. L. Yao, L. Y. Dai, H. Q. Zheng *et al.*, Rept. Prog. Phys. **84**(7), 076201 (2021)
[16] R. L. Workman *et al.* (Particle Data Group), PTEP **2022**, 083C (2022)
[17] J. J. Wu, S. Dulat and B. S. Zou, Phys. Rev. D **80**, 017503 (2009)
[18] J. J. Wu, S. Dulat, and B. S. Zou, Phys. Rev. C **81**, 045210 (2010)
[19] H. Zhang, J. Tulpan, M. Shrestha *et al.*, Phys. Rev. C **88**(3), 035205 (2013)
[20] H. Kamano, S. X. Nakamura, T. S. H. Lee *et al.*, Phys. Rev. C **92**(2), 025205 (2015)
[21] C. Helminen and D. O. Riska, Nucl. Phys. A **699**, 624-648 (2002)
[22] P. Gao J. J. Wu, and B. S. Zou, Phys. Rev. C **81**, 055203 (2010)
[23] J. J. Xie and L. S. Geng, Phys. Rev. D **95**(7), 074024 (2017)
[24] K. Moriya *et al.* (CLAS), Phys. Rev. C **87**(3), 035206 (2013)
[25] E. Wang, J. J. Xie, and E. Oset, Phys. Lett. B **753**, 526-532 (2016)
[26] L. J. Liu, E. Wang, J. J. Xie *et al.*, Phys. Rev. D **98**(11), 114017 (2018)
[27] K. P. Khemchandani, A. Martínez Torres, and J. A. Oller, Phys. Rev. C **100**(1), 015208 (2019)
[28] S. H. Kim, K. P. Khemchandani, A. Martinez Torres *et al.*, Phys. Rev. D **103**(11), 114017 (2021)
[29] M. Tanabashi *et al.* (Particle Data Group), Phys. Rev. D **98**(3), 030001 (2018)
[30] Y. L. Pan and F. L. Forman, Phys. Rev. Lett. **23**, 806-808 (1969)
[31] Y. L. Pan and F. L. Forman, Phys. Rev. Lett. **23**, 808-811 (1969)
[32] S. Chekanov *et al.* (ZEUS), Phys. Lett. B **591**, 7-22 (2004)
[33] I. Zychor, V. Koptev, M. Buscher *et al.*, Phys. Rev. Lett. **96**, 012002 (2006)
[34] Y. Oh, Phys. Rev. D **75**, 074002 (2007)
[35] C. Garcia-Recio, M. F. M. Lutz, and J. Nieves, Phys. Lett. B **582**, 49-54 (2004)
[36] Y. s. Oh, H. c. Kim, and S. H. Lee, Phys. Rev. D **69**, 094009 (2004)
[37] J. A. Oller, Eur. Phys. J. A **28**, 63-82 (2006)
[38] K. Hicks *et al.* (LEPS), Phys. Rev. Lett. **102**, 012501 (2009)
[39] E. Wang, J. J. Xie, W. H. Liang *et al.*, Phys. Rev. C **95**(1), 015205 (2017)
[40] N. C. Wei, A. C. Wang, F. Huang *et al.*, Phys. Rev. D **105**(9), 094017 (2022)

[41] A. C. Wang, N. C. Wei, and F. Huang, Phys. Rev. D **105**(3), 034017 (2022)
[42] A. C. Wang, W. L. Wang, and F. Huang, Phys. Rev. D **101**(7), 074025 (2020)
[43] J. J. Xie, E. Wang, and J. Nieves, Phys. Rev. C **89**(1), 015203 (2014)
[44] E. Wang, J. J. Xie, and J. Nieves, Phys. Rev. C **90**(6), 065203 (2014)
[45] D. Ronchen, M. Doring, F. Huang *et al*., Eur. Phys. J. A **49**, 44 (2013)
[46] T. A. Rijken, M. M. Nagels, and Y. Yamamoto, Prog. Theor. Phys. Suppl. **185**, 14-71 (2010)
[47] S. H. Kim, S. i. Nam, D. Jido *et al*., Phys. Rev. D **96**(1), 014003 (2017)
[48] V. G. J. Stoks and T. A. Rijken, Phys. Rev. C **59**, 3009-3020 (1999)
[49] Y. Zhang and F. Huang, Phys. Rev. C **103**(2), 025207 (2021)
[50] A. C. Wang, W. L. Wang, and F. Huang, Phys. Rev. C **98**(4), 045209 (2018)
[51] A. Donnachie and P. V. Landshoff, Phys. Lett. B **185**, 403 (1987)
[52] V. Y. Grishina, L. A. Kondratyuk, W. Cassing *et al*., Eur. Phys. J. A **25**, 141-150 (2005)
[53] Y. Y. Wang, L. J. Liu, E. Wang *et al*., Phys. Rev. D **95**(9), 096015 (2017)
[54] J. He, Nucl. Phys. A **927**, 24-35 (2014)
[55] M. Guidal, J. M. Laget, and M. Vanderhaeghen, Nucl. Phys. A **627**, 645-678 (1997)
[56] F. Huang, H. Haberzettl, and K. Nakayama, Phys. Rev. C **87**, 054004 (2013)